ACI MATERIALS JOURNAL TECHNICAL PAPER

Title no. 100-M58

Experimental Detection of Reinforcing Bar Corrosion Using Nondestructive Geophysical Techniques

by Susan S. Hubbard, Jieying Zhang, Paulo J. M. Monteiro, John E. Peterson, and Yoram Rubin

In this study, electrical impedance and ground-penetrating radar (GPR) methods were used to indicate corrosion of steel reinforcing bars embedded in a concrete block. Corrosion of the reinforcing bars was accelerated using an anodic polarization technique. Measurements were collected using both geophysical techniques before and after the corrosion experiments. Analysis of the geophysical measurements indicated the potential benefits and limitations of the two geophysical methods for assessing reinforcing bar corrosion. GPR methods have the advantage of providing a quick indication of alterations at the interface of the reinforcing bar surface and the surrounding concrete, and they have the potential to yield very high spatial resolution information. Although the electrical impedance techniques require longer measurement times and typically have lower spatial resolution than GPR techniques, these methods have the potential to provide valuable quantitative information about the corrosion process. Indications that corrosion had occurred were obtained independently and consistently from the two geophysical methods, and the observations were also corroborated by visual examination of the reinforcing bar corrosion state via destructive analysis of the experimental block. This first study suggests that these methods hold potential for direct and early detection of reinforcing bar corrosion, and that the combined use of the two methods for assessing reinforcing bar corrosion state merits further study.

Keywords: bridge deck; corrosion; deterioration; reinforced concrete; reinforcement bar.

INTRODUCTION

The U.S. Department of Transportation has declared that over 40% of the total number of bridges in the United States are classified as structurally deficient, with an associated estimated cost of repairs of billions of dollars.[1] One of the most significant contributors to bridge deficiencies and other concrete infrastructures is corrosion associated with reinforcing bars. Moisture and chloride ion exposure to uncoated reinforcing bars can initiate corrosion and yield expansive corrosion products, which can in turn accelerate the formation of cracks in the surrounding concrete. Early detection of reinforcing bar corrosion prior to the formation of the delamination cracks has the potential to significantly reduce the maintenance costs and extend the life of reinforced structures. As the reinforcing bars are embedded within concrete, however, early and noninvasive detection of corrosion is an extremely challenging task.

Visual, mechanical, electrical, and chemical techniques have been developed to detect reinforcing bar corrosion; several of these methods have been reviewed in the literature.[2] The conventional approaches for detection of reinforcing bar corrosion are often inadequate for field application for a variety of reasons: they can be invasive, the data acquisition procedures can be laborious, the procedures require lane closures, and many of the procedures do not quantify corrosion but instead indirectly detect the effects of reinforcing bar corrosion such as concrete cracking. For example, visual detection of delamination cracks or staining on the concrete surface is commonly used as an indicator of reinforcing bar corrosion, but this manifestation of reinforcing bar corrosion may only become apparent when the reinforced structure is in the process of being structurally weakened or has already deteriorated. Manual soundings of the pavement are quick and inexpensive but only detect delamination cracks rather than the extent of reinforcing bar corrosion. The half-cell electrical potential method provides a noninvasive approach for estimating the probability of corrosion; however, the measurements are sensitive to concrete conditions at the time of the survey. Electrolyte chemical tests involve assessing the composition of the concrete and inferring possible corrosion mechanisms from the analysis. Linear polarization and alternating current impedance methods all give an instantaneous indication of corrosion activity. Although these methods yield direct information about reinforcing bar corrosion, the methods typically require direct connection with the reinforcing bars and the measuring equipment, which renders in-place field measurements difficult under typical traffic conditions.

More recently, Monteiro, Morrison, and Frangos[3] investigated the use of a complex electrical impedance method for noninvasively providing information about the state of reinforcing bar corrosion. This method uses a four-electrode Wenner array to investigate the frequency-dependent change in electrical impedance. This technique has been successfully used to distinguish between reinforcing bars with different surface coatings[3] and to detect in-place reinforcing bar corrosion.[4,5] The technique is sensitive to reinforcing bar surface properties such as coatings and corrosion state, and does not require direct connection to the embedded reinforcing bar to acquire the measurement. The major drawback of the method is that the data acquisition procedure is time-consuming.

Ground-penetrating radar (GPR) is advantageous as a field tool in that it is nondestructive, it can yield data with very high spatial resolution (on the order of tenths of meters laterally), and the data can be acquired rapidly and even during traffic. Many studies have focused on uses of GPR for assisting transportation projects,[6-16] including measuring pavement thickness, detecting voids beneath pavements, detecting the location of reinforcing bars, detecting pavement structure

ACI Materials Journal, V. 100, No. 6, November-December 2003.
MS No. 02-469 received December 22, 2002, and reviewed under Institute publication policies. Pertinent discussion including authors' closure, if any, will be published in the September-October 2004 *ACI Materials Journal* if the discussion is received by June 1, 2004.

Susan S. Hubbard *is a staff scientist at Lawrence Berkeley National Laboratory, Berkeley, Calif. Her research interests include subsurface characterization using geophysical techniques.*

Jieying Zhang *is a postdoctoral researcher at the University of California at Berkeley, Berkeley, Calif. Her research interests include the development of complex resistivity methods for detecting reinforcing bar corrosion.*

ACI member **Paulo J. M. Monteiro** *is a professor of civil and environmental engineering at the University of California at Berkeley. His research interests include mathematical modeling and microstructure of concrete and testing methods.*

John E. Peterson *is a scientist at Lawrence Berkeley National Laboratory. His research interests include inversion of geophysical data for high-resolution subsurface imaging.*

Yoram Rubin *is a professor of civil and environmental engineering at the University of California at Berkeley. His research interests include the development of hydrological stochastic inverse approaches and subsurface characterization using geophysical data.*

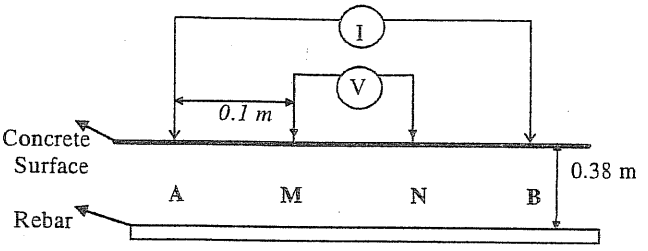

Fig. 1—Example of Wenner array showing four electrodes with spacing each of 10 cm.

changes, and mapping of underground utilities. Experimental and theoretical studies have been performed to understand the effects of frequency, concrete temperature, water content, concrete chloride content and concrete constituents on electromagnetic wave velocity and attenuation,[6,7] to develop GPR waveform inversion techniques,[7,8] and to understand the influence of delamination cracks on the GPR signal.[6,7,9,10,12,13] A comprehensive bibliography of GPR research dedicated to transportation issues is given by Morey.[14] A study by Narayanan, Hudson, and Kumke[12] marked the first attempt to investigate the use of GPR for early and direct detection of reinforcing bar corrosion prior to the formation of delamination fractures. In this study, comparisons of the variance of the GPR amplitude reflection strength was used in a field test as an indicator of reinforcing bar corrosion. This attempt met with success and recognized the need for further investigation of the technique using controlled experiments. In this study, the investigation of this approach under controlled conditions and in conjunction with another geophysical technique whose application has already been quantitatively demonstrated is continued.

In this study, the changes were investigated in both electrical impedance and in GPR measurements as corrosion of reinforced concrete was artificially accelerated. It was not attempted to directly invert the geophysical data for reinforcing bar-concrete properties. Instead, the electrical impedance and GPR attributes changes over time were investigated and these geophysical measurements were compared with each other and to the direct evidence of corrosion obtained by destructive analysis of the experimental concrete/reinforcing bar block. In the following two sections, background discussions associated with the two geophysical methods used in this study are presented. "Experimental approach" presents the experimental approach, and a discussion of the geophysical results and visual observations associated with the embedded reinforcing bars during the three corrosion experiments is given in "Experimental results and discussion," followed by the "Summary and conclusions."

RESEARCH SIGNIFICANCE

Analysis of the geophysical data collected in a time-lapse manner during accelerated reinforcing bar corrosion experiments suggests that both electrical impedance and GPR methods can be used to identify corrosion associated with steel reinforcing bars. An advantage of the GPR method for reinforcing bar corrosion detection over other techniques is that these data can be collected quickly during traffic, and GPR techniques can provide high resolution and multi-dimensional information in a nondestructive manner. Electrical impedance methods require more measurement time, but this method is also nondestructive and can yield quantitative information about the electrochemical processes. In practice, combining these two methods could potentially be very useful for early detection of reinforcing bar corrosion. For example, the corroding zones could be quickly identified by GPR followed by a more precise quantification of the corrosion state using electrical impedance techniques. In this first study, we investigated the potential that the two geophysical methods hold individually for indicating reinforcing bar corrosion during accelerated corrosion experiments.

Electrical impedance background

Electrical impedance techniques measure the interfacial impedance spectrum at the interface between the reinforcing bar and concrete. The frequency-dependent resistivity mapping of the subsurface, also known as the induced polarization (IP) method, has been applied successfully by geophysicists in the discovery of mineral deposits,[17] and the application of this technique for reinforcing bar corrosion has been demonstrated by Montiero, Morrison, Frangos[3] and reviewed by Swiat et al.[2] The fundamental principle underlying the approach is that there is a relationship between the chemical state of the interface between the reinforcing bar and the surrounding concrete and the electrical impedance it offers to an impressed alternating current. The corrosion state of the reinforcing bar can thus be investigated using complex resistivity measurements acquired by electrodes placed on the concrete surface (Fig. 1). Because the embedded reinforcing bar and the concrete matrix have distinct electrical resistive behaviors, when current is injected into the concrete matrix, the current distribution is distorted by the presence of the reinforcing bar, and the measured voltage response reflects this distortion. The distortion of both the resistivity moduli and phase as a function of frequency can be analyzed to investigate corrosion processes. For instance, the corrosion resistance can be derived from the difference in the measured impedance at low frequency and high frequencies, and the capacitance of the double layer (between the reinforcing bar and the concrete) can also be obtained via analysis of the frequency-dependent impedance spectra.

The impedance mapping conducted on the concrete surface depends on the interface impedance, but it is also strongly influenced by the resistivity of concrete, the depth and diameter of the reinforcing bar, and the electrode configuration, all of which must be factored in when measuring the response of the reinforcing bar and concrete interface. Mathematical inverse modeling[18] has shown that direct quantitative estimates of corrosion parameters can be uniquely obtained from the complex measurements. At this stage, however, the interpretation of the corrosion activity is

based on observation of the changes in the measured modulus and phase as a function of frequency.

The Wenner array (refer to Fig. 1) used in this work is only one of a variety of electrode configurations that may be used. The voltage V between the two electrodes is related to the current I on the other two by an expression of the form $V = I\rho/k(r)$, where k is a geometric factor, which is equal to $2\pi a$ (a, the spacing of electrodes) for the Wenner array, and ρ is the electrical resistivity. The resistivity obtained from this expression is a complex number when alternating current is used and is herein referred to as the measured impedance.

GPR background

GPR methods use electromagnetic energy, typically at frequencies of 50 to 1200 MHz, to probe the subsurface. A GPR system consists of an impulse generator, which repeatedly sends a particular voltage and frequency source to a transmitting antenna *Tx*. A signal propagates from the transmitting antenna through the earth and is reflected, scattered, and attenuated; the receiving antenna *Rx* subsequently records the modified signal. The reflected signal R that is returned to the receiving antenna is typically displayed as a waveform of voltage variations as a function of time. The depth of penetration of the GPR signal is a function of the radar system parameters, target parameters, and the electromagnetic properties of the materials being investigated, and can be calculated using a radar range equation.[17] In general, GPR signal penetration is lower when higher GPR frequencies are used or in the presence of electrically conductive materials.

The most common GPR acquisition mode is common-offset reflection, which involves collecting one trace per surface location from a transmitter-receiver antenna pair that has a fixed separation distance S as the antenna pair is moved along the ground/concrete surface or from an elevated position above the ground surface (Fig. 2). Data collected in this mode are typically displayed as wiggle-trace profiles, with the distance that the radar antenna pair has traversed on the horizontal axis and two-way signal travel-time on the vertical axis. In addition to reflected energy, other events arrive at the receiving antenna from the transmitting antenna including the air wave and the ground wave, as shown in Fig. 2.[19] Using a standard display, GPR data often provide a cross-sectional image of the near subsurface along the GPR traverse that illustrates boundaries with different electromagnetic properties. In addition to using these reflections to map subsurface features, information about the subsurface layer or interface properties can be extracted from the GPR waveforms.

The propagation velocity and amplitude of the recorded electromagnetic waveform can be analyzed to infer subsurface properties or changes in these properties. For low loss materials such as concrete with low to medium salt and moisture content, with the high frequencies that are typically used for assessment of pavements (~ 1GHz), and neglecting dispersion, the velocity v of the electromagnetic wave primarily depends on the relative permittivity or equivalently the dielectric constant κ of the material according to[19]

$$v \approx \frac{c}{\sqrt{\kappa}} \tag{1}$$

where c is the speed of light (300 mm/ns). The dielectric constant of air is approximately 1, of water is approximately

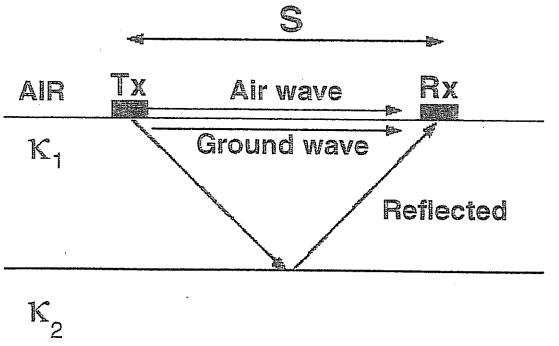

Fig. 2—Schematic showing surface GPR common offset arrivals between GPR transmitting antenna Tx *and receiving antenna* Rx*, which are separated by a distance* S*. Arrivals include the air wave, ground wave, and reflected events that occur when there is contrast of dielectric constant (κ) across a boundary, such as at reinforcing bar-concrete interface.*

80, and of dry natural or engineered materials of approximately 4 to 10. Thus, dielectric constants of both natural and engineered materials vary primarily as a function of water content but are also affected by variations in porosity, material constituency, temperature, pore fluid salinity, and particle or pore shape.

At interfaces between materials of different electromagnetic properties, part of the signal travels through the interface to the next layer and the rest of the signal is returned toward the surface and is recorded by the receiving antenna. The magnitude of the amplitude that is returned to the surface is a function of the electromagnetic impedance of the two materials: the greater the contrast, the stronger the GPR reflection. For low loss materials and at high GPR frequencies, the reflection coefficient R quantifies the magnitude of the returned signal amplitude of the reflected wave as a function of the values of the upper (κ_1) and lower (κ_2) material dielectric constants[20]

$$R = \frac{\sqrt{\kappa_1} - \sqrt{\kappa_2}}{\sqrt{\kappa_1} + \sqrt{\kappa_2}} \tag{2}$$

Using Eq. (2), the amplitude of the recorded event can be analyzed to obtain information about boundaries where there are changes in dielectric constant, such as at the concrete-reinforcing bar interface.

To test the utility of using GPR information for early detection of reinforcing bar corrosion, the changes in GPR attributes over time during several accelerated reinforcing bar corrosion experiments were investigated. Changes in factors associated with GPR velocity and amplitude were considered. Small changes in concrete moisture that occurred as a part of the accelerated corrosion experimental process (as described in "Experimental procedure") may slightly decrease the GPR velocity. Scattering of the wave by irregularities at the surface of a corroded reinforcing bar, or decreases in the reinforcing bar dielectric constant (κ_2 in Eq. (2)) with increasing corrosion,[11] could both contribute to decreased GPR amplitudes. The GPR amplitude data was analyzed in the frequency domain using the amplitudes obtained from Fourier transformation of the data $A(\omega)$ where ω denotes the frequency.[21] In this study, the energy spectrum obtained from these amplitudes as a spectral density function $S(\omega)$ is expressed as

$$S(k) = \langle A(\omega)A(\omega)^* \rangle \tag{3}$$

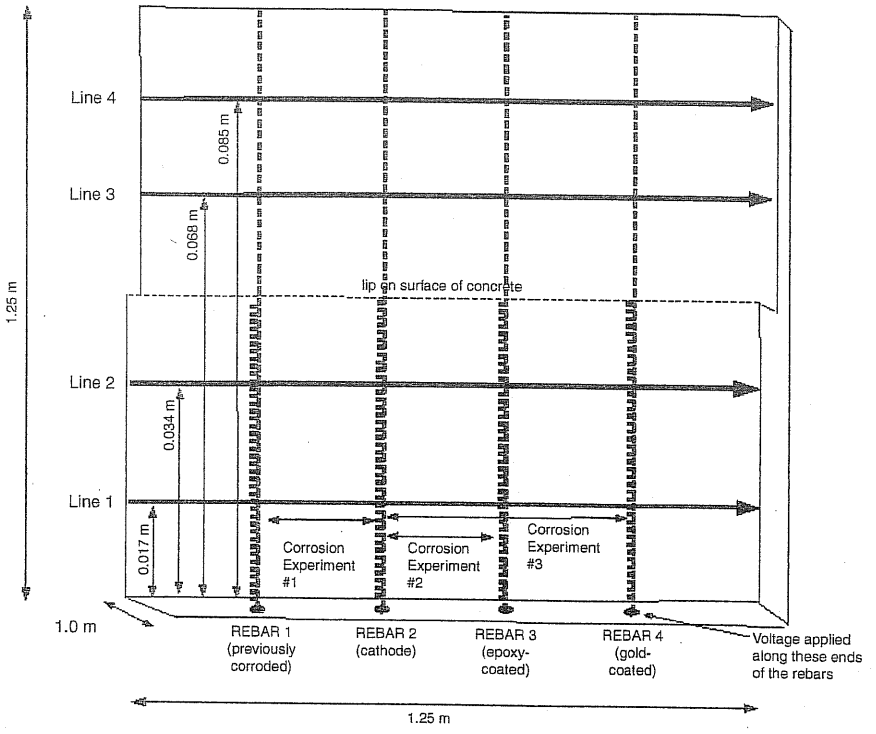

Fig. 3—Plan view map of concrete block and four buried reinforcing bars (dashed lines). Thick lines with arrows indicate location of the four surface GPR traverses that were performed before and after each corrosion experiment, and thick hatched lines show the locations of the four Wenner arrays that were used to collect electrical impedance data during each experiment.

where the asterisk denotes the complex conjugate, and $\langle\ \rangle$ denotes the expected value.[22]

EXPERIMENTAL APPROACH

Experimental configuration

The experiments were conducted over a single concrete slab of dimensions 1.25 x 1.0 x 0.25 m that was embedded with four parallel reinforcing bars as illustrated in Fig. 3. The concrete mixture proportions were 403 kg/m^3 ASTM Type II cement, 71 kg/m^3 pozzolan, 193 kg/m^3 water, 608 kg/m^3 pea gravel, 914 kg/m^3 top sand, and 156 kg/m^3 blended sand. A lip in the concrete surface was designed to position the reinforcing bars at two different depths below the concrete slab surface: 0.038 and 0.019 m (Fig. 3). The impedance measurements were acquired only on the section where the reinforcing bars were located 0.038 m beneath the top of the concrete slab to limit the number of variables. Although the reinforcing bars were all 0.00127 m in diameter, they differed in their surface composition. The experiments included testing corrosion effects on:

- a reinforcing bar that had previously been subjected to corrosion by exposure to water for 24 h (No. 1);
- a reinforcing bar that had been sandblasted clean (No. 2);
- a reinforcing bar with an electrically insulating epoxy coating that had been manually applied (No. 3); and
- a reinforcing bar that had been sandblasted, nickel electroplated, and then gold electroplated (No. 4).

The four bars were designed to represent different reinforcing bar-concrete interfaces: reinforcing bar No. 1 represents a corroded surface, reinforcing bar No. 2 represents a passivated surface, the epoxy-coated surface of reinforcing bar No. 3 was designed to provide capacitive coupling to the concrete, and the gold surface coating of reinforcing bar No. 4 was designed to render the reinforcing bar surface chemically inert under natural conditions.

Experimental procedure

Three accelerated corrosion experiments were conducted between different pairs of the four reinforcing bars. An anodic polarization technique was used to accelerate corrosion in the reinforcing bars, whereby a 240 direct current voltage, provided by a rectifier, was introduced to the ends of the reinforcing bars and current was impressed between the reinforcing bar pairs for ten days for each experiment. To ensure better contact, the concrete block was moistened prior to each experiment and was kept moist during the experiments by rewetting every two days and covering the concrete slab with a moist burlap. Three accelerations were applied to reinforcing bars No. 1, 3, and 4 in sequence, with reinforcing bar No. 2 always serving as the cathode (Table 1). The current flows in the accelerations were assessed frequently by measurement of the DC resistivity between the two reinforcing bars serving as the anode and cathode. The voltage V between two reinforcing bars is given by

$$V = \varepsilon_{anode} + I \times R_{\Omega concrete} \varepsilon_{cathode} \quad (4)$$

where ε_{anode} and $\varepsilon_{cathode}$ are the potential drop of the reinforcing bars, $R_{\Omega concrete}$ is the resistance of the concrete between, and I is the current flow. The total Ohmic potential change $I \times R_{\Omega concrete}$ is orders of magnitude larger than $\varepsilon_{cathode}$ and ε_{anode}.[23] As such, Eq. (4) can be simplified to $V = I \times R_{\Omega concrete}$ and the current flows can be approximately calculated. The current flow calculated in this manner for the

Table 1—Description of experimental chronology and parameters

Experiment	Anode reinforcing bar	Anode coating	Cathode reinforcing bar	Corrosion rate (A/m^2)	Date of prior GPR data collection	Date of prior electrical impedance collection	Beginning data of 10-day corrosion experiment	Date of posterior GPR data collection	Date of posterior electrical impedance collection
1	No. 1	Corroded	No. 2	2.60	12/21/00	12/24/00	12/24/99	01/03/00	01/03/00
2	No. 3	Epoxy	No. 2	0.372	12/21/00	01/04/00	01/04/00	01/14/00	01/14/00
3	No. 4	Gold	No. 2	1.10	01/07/00	02/07/00	02/07/00	02/18/00	02/18/00

three experiments reported herein are indicative of corrosion rate and given in Table 1.

To test the corrosion detectability of different types of reinforcing bars using the geophysical techniques, both electrical impedance and GPR data were collected in a time-lapse manner relative to the three accelerated reinforcing bar corrosion experiments. Before each corrosion experiment was performed, prior GPR and electrical impedance data sets were collected. For each experiment, the concrete slab was then wetted to facilitate the reinforcing bar corrosion process, and the voltage was induced for 10 days. After concluding each acceleration experiment, the posterior geophysical data sets were collected. Analysis of the difference in geophysical attributes obtained prior and subsequent to the corrosion experiment was used to indicate if corrosion had occurred. The dates of the geophysical acquisition campaigns relative to the corrosion experiments are given in Table 1.

Wenner arrays (Fig. 1) were used to measure the complex resistivity spectra. With this geometry, the electrodes were placed on the concrete surface directly above the reinforcing bar in the parallel direction with an electrode spacing of 0.01 m over the section of the concrete block that had a cover of 0.038 m. Figure 3 shows the location of the Wenner arrays on the concrete surface; all arrays were collected during each experiment. The measurement followed the procedure described by Zhang et al.[4] A sinusoidal current with a magnitude of 0.1 mA was injected through Electrodes A and B, and the voltage was measured between Electrodes M and N (Fig. 1). A complex resistivity spectrum was obtained by the ratio of the measured voltage V, including both a modulus and phase shift angle, to the input current I, multiplied with a geometry factor $k = 2\pi a$, where a is the electrode spacing.

GPR data were also collected before and after the corrosion experiments. Each GPR data acquisition campaign (that is, before and after each experiment) included collection of four 1200 MHz GPR lines in a direction perpendicular to the reinforcing bar axes as shown in Fig. 3. The GPR data were collected with a measurement spacing of 0.01 m, a sampling interval of 50 picoseconds, and by stacking the data at each sampling location 16 times. Figure 4(a) schematically shows how the transmitter-receiver antennae pair was pulled along the concrete slab surface in a direction perpendicular to the four reinforcing bars to collect a single GPR line. As the antennae pair is directly over the reinforcing bar axis, the travel time of the signal to the reinforcing bar is shortest; as the antenna pair moves away from the reinforcing bar axis, the travel time increases. This movement of the antennae pair over the reflector yields a reflection hyperbola on the GPR profile image as illustrated in Figure 4(b). In this display, the (constant) air and ground wave arrivals (refer to Fig. 1) have been suppressed by subtracting out the mean trace in the line. The low frequency (< 100 MHz) noisy portion of the signal has been removed by filtering, and no amplitude gains have been applied. The GPR profile

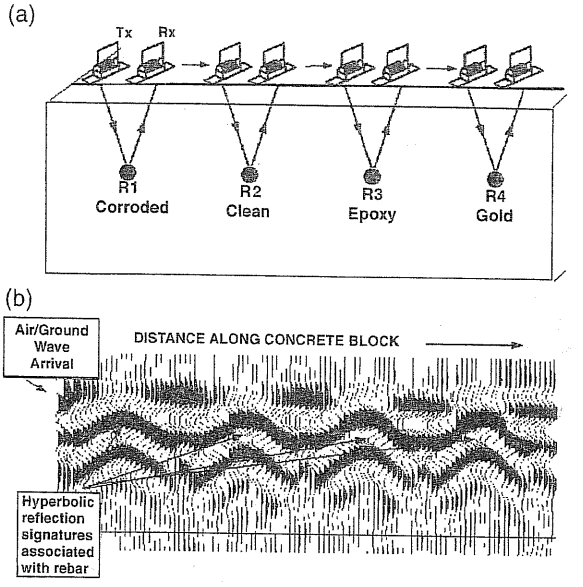

Fig. 4—(a) Schematic showing collection of surface GPR data over four buried reinforcing bars. Tx *is transmitter and* Rx *is receiving antenna; and (b) Example GPR profile collected over the four buried reinforcing bars using 1200 MHz GPR system prior to corrosion experiment.*

predominantly displays the hyperbolic response of the signal travel time as the transmitter/receiver pair traverse over the four embedded reinforcing bars. The location of the reinforcing bar at the apex of the hyperbolas was clearly identifiable on all of the GPR profiles.

After the experiments were completed, the concrete block was carefully autopsied to observe the magnitude of corrosion at each reinforcing bar location. In the following discussion, the geophysical observations associated with each geophysical method during each of the three experiments are reported. The responses of the two techniques are then compared with each other and also with visual observations made on the destructed experimental block.

EXPERIMENTAL RESULTS AND DISCUSSION

Assessment of initial conditions

The reinforcing bar embedded in the concrete slab influences both the GPR and electrical impedance measurements. The dramatic difference between the electromagnetic properties of the concrete and the reinforcing bar produced a large GPR reflection coefficient at the concrete/reinforcing bar interface as described by Eq. (2) and illustrated in Fig. 4(b). The analysis of GPR data collected at only one point in time, such as the prior data set shown in Fig. 4(b), suggested, however, that GPR information was not sufficient to distinguish between the four different coating materials of the reinforcing bars embedded within the concrete slab.

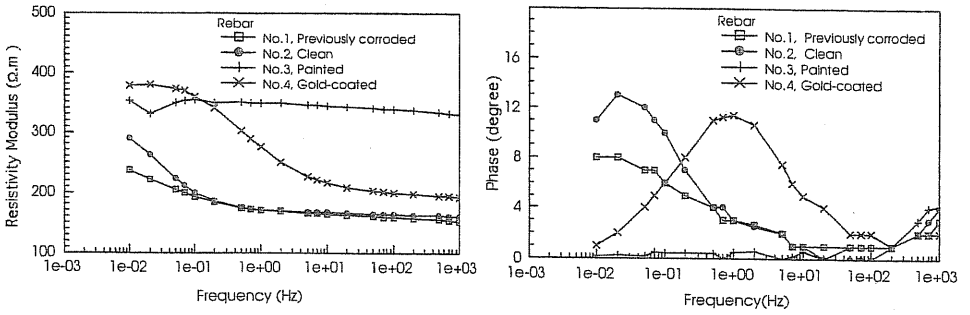

Fig. 5—Complex impedance measurements associated with initial conditions of reinforcing bar including modulus versus frequency and phase versus frequency.

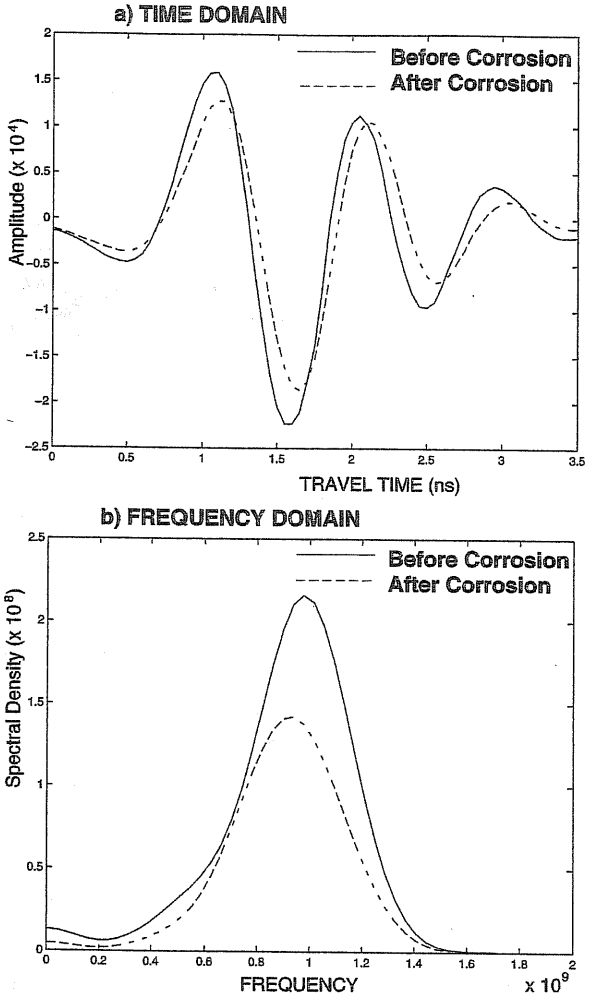

Fig. 6—Average GPR: (a) travel time; and (b) spectral amplitude calculated at reflection hyperbola apex recorded at Reinforcing Bar No. 1, along GPR Line 1, and during Experiment 1.

In contrast, the impedance responses varied for the different initial surface reinforcing bar materials or different reinforcing bar-concrete interface conditions. Figure 5 illustrates the initial complex resistivity spectra obtained using the impedance measurements associated with the four different reinforcing bars. The resistivity modulus and peak phase measurements as functions of frequency are different for each reinforcing bar condition. The frequency where the phase angle reaches the maximum value is often referred to as the critical frequency *fc* and has the largest value for the gold-coated reinforcing bar No. 4. Compared with reinforcing bar No.1, reinforcing bar No. 2 shows a higher phase shift angle due to its higher corrosion resistance, which is in agreement with the observations of Gu et al.[24] The frequency dependency is not apparent on the phase responses associated with the epoxy-coated reinforcing bar No. 3, and the phase shift is almost zero for all frequencies less than 100 Hz. The differences in the electrical responses indicate the potential of this method for providing quantitative information about the chemical state of the reinforcing bar-concrete interface and thus about the corrosion state.

Experimental results

All four GPR lines and four Wenner arrays shown in Fig. 3 were collected before and after each of the three experiments (Table 1). The differences in all GPR attributes for all lines during each experiment were calculated, and the GPR signal was most modified at the location of the reinforcing bar serving as the anode for the particular experiment, and was also closest to the location of the applied voltage. Thus, for most of the following discussion, only the results obtained along GPR line 1 (refer to Fig. 3) are discussed, which is closest to where the voltage was applied to the four reinforcing bars during the accelerated corrosion experiments. Those measurements were compared with the complex resistivity data collected over the reinforcing bar serving as the cathode for that experiment. The results of the geophysical data analysis are discussed individually for each experiment as follows, and these results are compared with the visual observations of the reinforcing bar corrosion state made on the autopsied concrete block after the experiments had concluded.

Experiment No. 1—Reinforcing Bar No. 1, which had previously been subjected to corrosion,[3] served as the anode for corrosion Experiment No. 1. GPR and electrical impedance data sets were collected prior and subsequent to the experiment, as shown in Table 1. To assess the changes in GPR attributes associated with this and all subsequent corrosion experiments, differences of the travel times and spectral amplitudes were calculated.[3] For this calculation, the average attribute associated with the three traces located at the apex of the reflection hyperbola associated with the reinforcing bar serving as the anode during the experiment (refer to Fig. 4(b)) was used. The average GPR travel time and amplitude responses that occurred before and after this experiment at reinforcing bar No. 1 are illustrated in Fig. 6. Figure 6(a) shows that the travel time is longer (or velocity is slower) for the data collected after the corrosion experiment, and Fig. 6(b) shows that the spectral amplitude associated with those waveforms is decreased relative to the data collected prior to the experiment. To calculate the travel time shift associated with the experiment, the time difference between the first

Table 2—Changes in GPR and complex electrical attributes acquired prior and subsequent to three different corrosion acceleration experiments

Experiment	Reinforcing bar	Radar line	GPR*	GPR†	Electrical‡	Electrical§
1	1	1	0.1	1.49	7.1	70
2	3	1	0.1	1.14	0.3	5
3	4	1	0.0	2.08	5.5	111

*Time shift (posterior-prior, ns).
†Spectral amplitude ratio.
‡Peak phase shift (before-after, degrees).
§Maximum decrease in modulus (before-after, Ohm-m).

trough (the center of the first negative amplitude peak) and the third trough in the prior signal was calculated, and the difference calculated over the same portion of the wavelet using the posterior data was subtracted from it. This time shift is reported in Table 2. The change in GPR spectral amplitudes as a ratio of the prior spectral amplitude to the posterior spectral amplitude was assessed. For example, if there was no change in spectral amplitude during the course of the experiment, the ratio of the GPR amplitude collected acquired prior to the experiment relative to the posterior data would be 1. If the GPR amplitudes decreased during the experiment, then the ratio becomes larger. Ratios substantially greater than 1 indicate a large decrease in GPR amplitudes over the course of the corrosion experiment.

Table 2 lists both the time shift and the amplitude ratio associated with the GPR imaging over Reinforcing Bar No. 1 during Experiment No. 1. These data revealed that a small time shift and a significant reduction in amplitude occurred during the experiment. Analysis of all the data collected over the entire concrete block during this experiment (that is, over reinforcing bar No. 1 as well as over the three other reinforcing bars using all 4 GPR lines) showed similar small time shifts, suggesting that the small time shift was not a localized phenomena. This time shift is interpreted to be caused by concrete wetting that was performed during the experiment. The significant decrease in amplitude, however, was only associated with the signals over reinforcing bar No. 1 and along GPR Line 1. As corrosion occurs, the roughness of the reinforcing bar-concrete interface is expected to increase, which may serve to scatter and thus attenuate the radar wave. Additionally, changes in the chemical state of the cement in the vicinity may result in a change in reflection coefficient following.[2] The GPR amplitude decrease observed in this experiment is interpreted to be associated with corrosion that occurred during the experiment and along the length of Reinforcing Bar No. 1.

Figure 7 illustrates the changes in the complex electrical resistivity parameters at reinforcing bar No. 1 during Experiment No. 1. Both the resistivity modulus curve and the phase shift angle curve were changed during the course of the corrosion experiment. The modulus of the data obtained after the experiment was significantly lower relative to that obtained prior to the experiment, especially at the low frequency end of the spectrum. Additionally, the peak phase was reduced to almost zero. Table 2 lists the change of the peak phase shift and the maximum measured resistivity modulus drop associated with the corrosion acceleration experiment at Reinforcing bar No. 1. The changes in both phase and modulus associated with Reinforcing Bar No. 1 and Experiment No. 1 are significant, and these

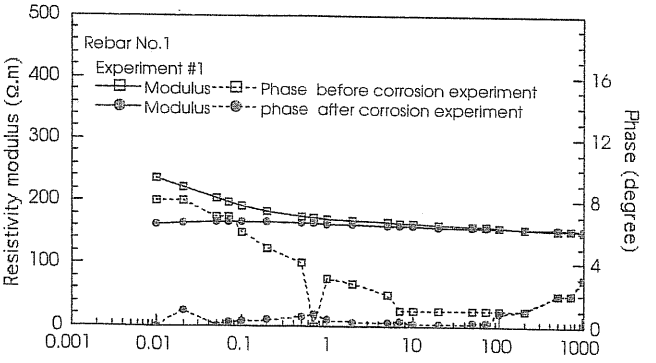

Fig. 7—Complex impedance parameters collected before and after corrosion Experiment No. 1 and at Reinforcing Bar No. 1.

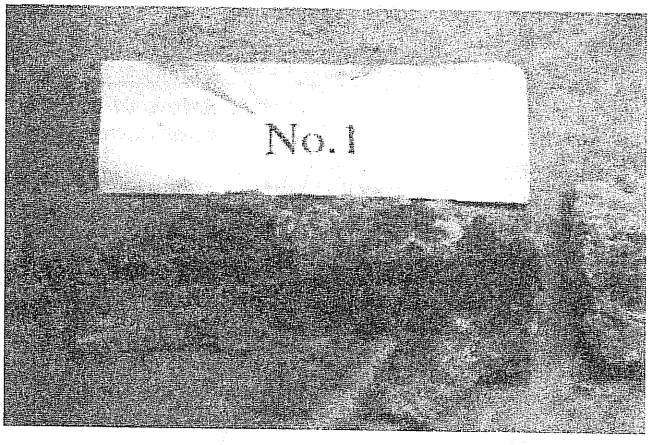

Fig. 8—Destructive analysis of concrete block at Reinforcing Bar No. 1 showing stained concrete that surrounded Reinforcing Bar No. 1, which is indication of reinforcing bar corrosion.

changes are interpreted to be associated with reinforcing bar corrosion that occurred during the acceleration experiment.

The changes detected by electrical impedance and GPR measurements were confirmed by the visual observation on both the exterior and the interior of the concrete block. On the concrete surface, a long thin crack formed along the direction of Reinforcing Bar No. 1 directly above the reinforcing bar. In the same vicinity but after block autopsy, corrosion-related red staining was also observed directly adjacent to the reinforcing bar, as shown by Fig. 8.

Experiment No. 2—Reinforcing Bar No. 3, which had an epoxy coating, served as the anode for Experiment No. 2. Again, both GPR and electrical impedance data were collected before and after the experiment as shown in Table 1. The GPR responses are shown in Fig. 9, and the time and frequency domain GPR attribute differences were calculated as described previously and are listed in Table 2. As with Experiment No. 1, there are small but observable changes in the GPR travel times that are attributed to increased concrete moisture associated with the corrosion experimental procedure. This small time shift was observed on all of the other GPR data collected during the experiment as is expected, as the entire concrete block was wetted. The GPR amplitude value, however, showed very little change over the course of this experiment. The lack of change in GPR spectral amplitude

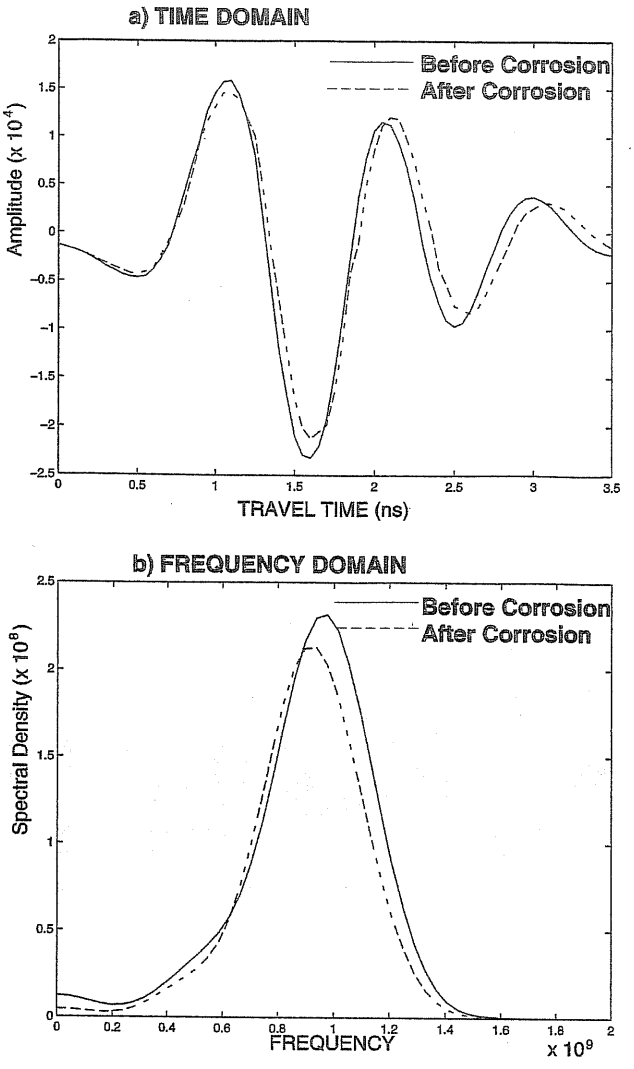

Fig. 9—Average GPR: a) time shift; and b) spectral amplitude reflection hyperbola apex recorded at Reinforcing Bar No. 3, along GPR Line 1, and during Experiment No. 2.

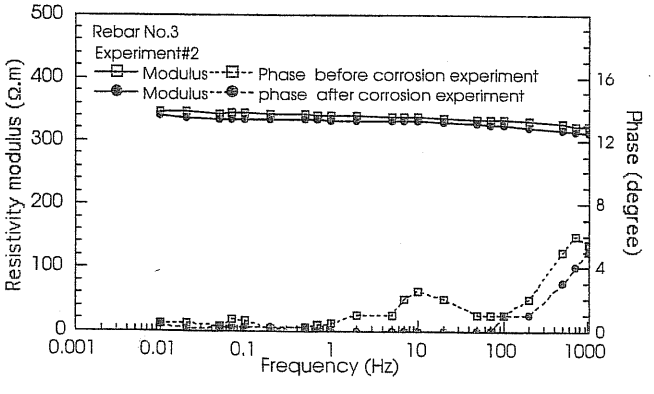

Fig. 10—Complex impedance parameters collected before and after corrosion Experiment No. 2 and Reinforcing Bar No. 3.

suggested that there has been insignificant reinforcing bar corrosion at this location.

The data collected using the electrical impedance technique also yielded similar null results for this experiment. As seen from the resistivity spectra shown in Fig. 10 and reported in Table 2, there was almost no change in the resistivity

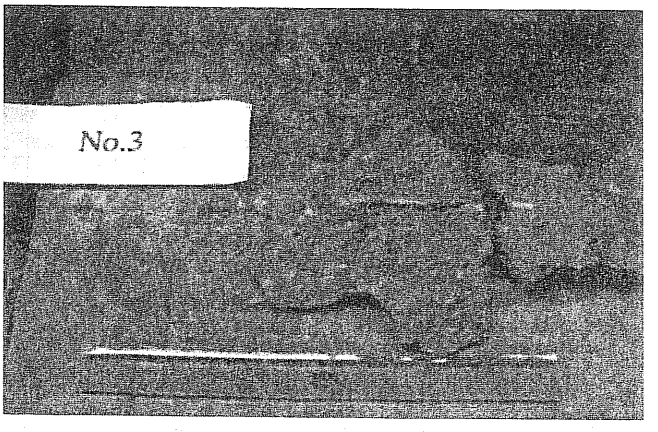

Fig. 11—Destructive analysis of concrete block at Reinforcing Bar No. 3, which revealed no indication of reinforcing bar corrosion at that location.

modulus nor in the phase shift as a function of frequency, indicating that there was insignificant corrosion along this reinforcing bar. Under the same voltage applied for all experiments, Table 1 shows that the corrosion current induced was negligibly small due to the high resistive epoxy paint surrounding Reinforcing Bar No.3.

The geophysical observations were corroborated by destructive analysis of the concrete block. Figure 11 shows the concrete surrounding Reinforcing Bar No. 3 and illustrates that no corrosion occurred in the vicinity of this epoxy-coated reinforcing bar as had been suggested by the geophysical responses.

Experiment No. 3—In the final experiment, Reinforcing Bar No. 4 served as the anode. Figure 12 illustrates the variations in time and frequency domain responses for this experiment, and the changes in GPR attributes are quantified in Table 2. The figures and calculated differences suggest that the GPR amplitudes have been substantially modified during the course of the experiment. Because the block was moist during both the prior and the posterior GPR data acquisition campaigns, there was no significant shift in the travel time associated with this experiment. The resistivity data, shown in Fig. 13 and reported in Table 2, reveal dramatic changes in the resistivity modulus and phase. Although Reinforcing Bar No. 4 was gold-coated and not susceptible to corrosion under natural conditions, impression of current within this gold-coated reinforcing bar may have caused cracking and oxidation of the gold surface coating and subsequent corrosion of the reinforcing bar. During this experiment, the dramatic alterations of the geophysical signatures suggested that there was indeed a change in surface properties of the gold-coated reinforcing bar and concomitant reinforcing bar corrosion.

The significant changes observed using both geophysical techniques were again corroborated by the visual observations made during destructive analysis of the block. During the block autopsy, it was found that the gold coating had failed and that reinforcing bar corrosion had occurred at this location.

Spatial variations in corrosion

In the three experiments discussed previously, changes in the geophysical attributes that were presented in Table 2 were only those measurements made closest to the application of the applied reinforcing bar voltage and at the location of the anode reinforcing bar. Because the GPR data were collected along four lines during each experiment, these data

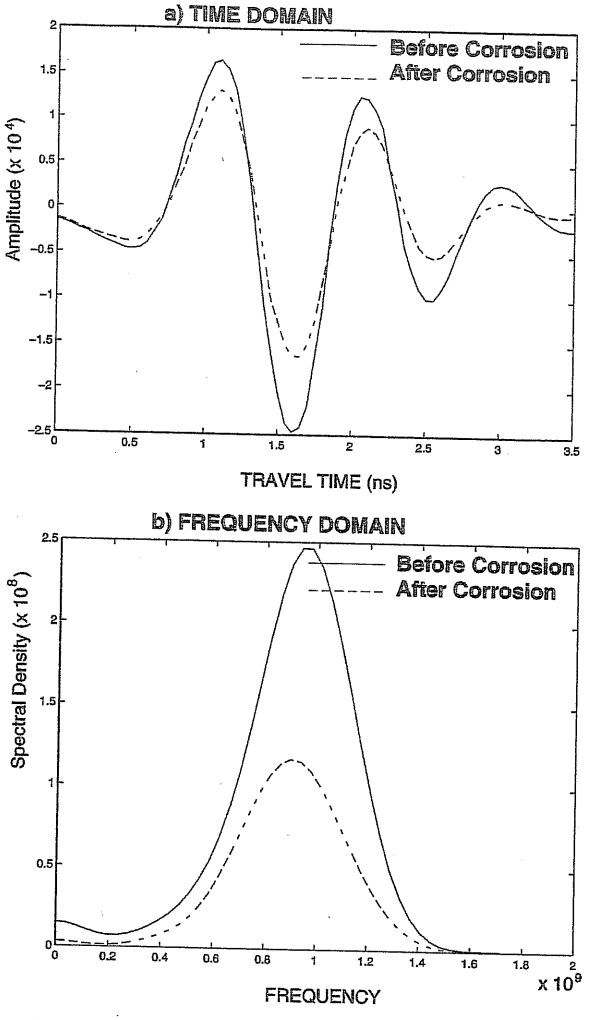

Fig. 12—Average GPR: a) travel times; and b) spectral amplitudes at reflection hyperbola apex recorded at Reinforcing Bar No. 4, along GPR Line 1, and during Experiment No. 3.

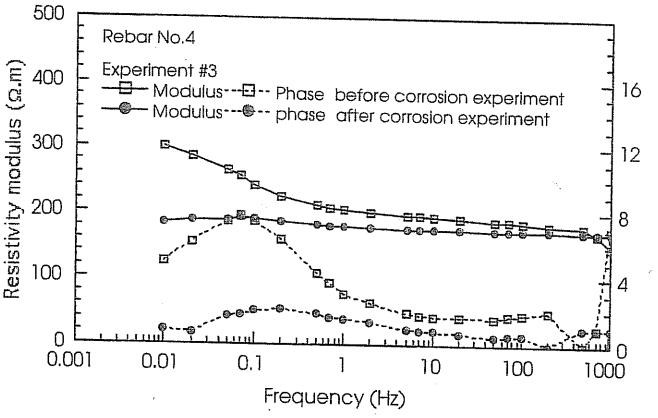

Fig. 13—Complex impedance parameters collected before and after corrosion experiment No. 3 at reinforcing bar No. 4.

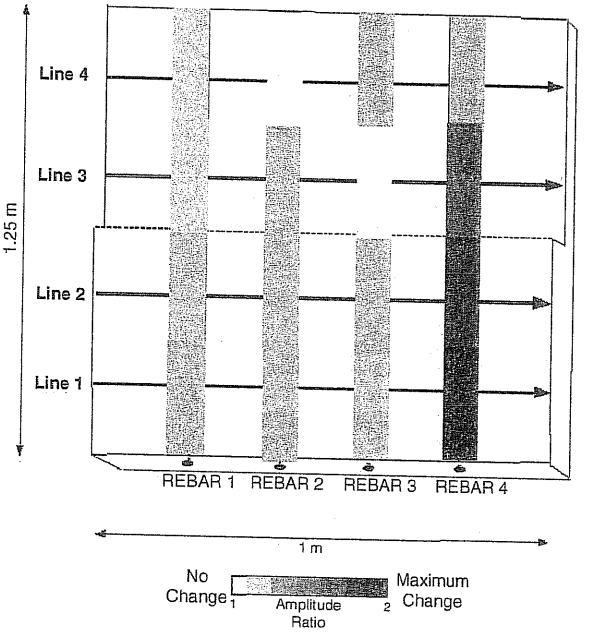

Fig. 14—Spatial distribution of spectral amplitudes associated with Experiment No. 3, which was designed to corrode Reinforcing Bar No. 4. Observe that greatest changes occur along Reinforcing Bar No. 4 closest to location of applied voltage. Minor changes in amplitude ratios associated with other reinforcing bars during this experiment are interpreted to be due to continuing corrosion of other reinforcing bars associated with Experiments No. 1 and 2.

can be used to investigate the changes in GPR responses over the entire concrete block. Figure 14 displays the modifications of the GPR amplitude over all reinforcing bars during Experiment No. 3, which was designed to corrode Reinforcing Bar No. 4. This example illustrates that the GPR signal was most attenuated (the amplitude ratio most increased) along reinforcing bar No. 4, and the modifications were greatest closest to the location of applied voltage. The figure also indicates that there are small changes in other reinforcing bars between the data collected prior to and subsequent to the corrosion experiment, which could be due to stray current associated with Experiment No. 3 or due to continuing corrosion induced during the previous acceleration experiments (No. 1 and No. 2). This figure illustrates the potential of the GPR methods to provide multidimensional and high spatial information in a noninvasive manner.

SUMMARY AND CONCLUSIONS

The experimental results indicated that the electrical impedance and GPR measurements acquired in time-lapse manner on the concrete surface have the potential to detect changes in the corrosion state of the reinforcing bar embedded beneath. Both methods indicated that Reinforcing Bar No. 3, the epoxy-coated reinforcing bar, experienced the least amount of corrosion during the acceleration Experiment No. 2. Both geophysical techniques also indicated that the most dramatic changes were associated with Reinforcing Bar No. 4 (during Experiment No. 3), which was the reinforcing bar with the cracked gold coating, followed by Reinforcing Bar No. 1 (during Experiment No. 1), which was the reinforcing bar that had previously been subjected to corrosion. These indications were corroborated by visual examination of the destructed concrete experimental block.

The measurements suggest that GPR amplitude data, collected in a time-lapse mode, have the potential to indicate if corrosion has occurred, and that the electrical impedance methods may be able to provide more quantitative information about the corrosion process. To quantitatively establish the relation between acquired signals and corrosion information,

however, further study is necessary to quantify how other parameters (such as concrete wetness, chlorides, and cracks) influence the geophysical signatures. Furthermore, more study is needed to investigate how the two different methods can be used together to develop the most accurate and efficient approach for non-invasively detecting reinforcing bar corrosion, and to test the approach at the field scale. In this first experiment, the authors strove only to illustrate the potential that these two different, novel, and noninvasive methods have for detecting reinforcing bar corrosion rather than to quantify the corrosion magnitude. This study suggests that these methods hold potential for direct and early detection of reinforcing bar corrosion, and that the combined use of the two methods merits further study at both the laboratory and the field scales.

ACKNOWLEDGMENTS

The GPR processing was carried out at the Center for Computational Seismology (CCS) at Lawrence Berkeley National Laboratory, Berkeley, Calif.

REFERENCES

1. Dunker, K. F., and Rabbat, B. G., "Highway Bridge Type and Performance Patterns," *Journal of Performance of Constructed Facilities*, V. 4, No. 3, 1990, pp. 161-173.

2. Swiat, E.; Young, W.; Pajak, J.; Funahashi, M.; Burke, D.; and Wagner, J., "State of the Art Report: Corrosion of Steel in Concrete," *Report ORNL NRC-LTR* 93-2, Oak Ridge National Laboratory, Oak Ridge, Tenn., 1993, 96 pp.

3. Monteiro, P. J. M.; Morrison, F.; and Frangos, W., "Nondestructive Measurement of Corrosion State of Reinforcing Steel in Concrete," *ACI Materials Journal*, V. 95, No. 6, Nov.-Dec. 1998, pp. 704-709.

4. Zhang, J.; Monteiro, P. J. M.; and Morrison, F. H., "Noninvasive Surface Measurement of Corrosion Impedance of Reinforcing Bar in Concrete—Part I: Experimental Results," *ACI Materials Journal*, V. 98, No. 2, Mar.-Apr. 2001, pp. 116-125.

5. Zhang, J., "Noninvasive Surface Measurement of the Corrosion Impedance of Reinforcing Bar in Concrete," PhD dissertation, University of California at Berkeley, Calif., Aug. 2001, 173 pp.

6. Halabe, U. B.; Sotoodehnia, A.; Maser, K. R.; and Kausel, E. A., "Modeling of the Electromagnetic Properties of Concrete," *ACI Materials Journal*, V. 90, No. 6, Nov.-Dec. 1993, pp. 552-563.

7. Halabe, U. B.; Maser, K. R.; and Kausel, E. A., "Condition Assessment of Reinforced Concrete Structures Using Electromagnetic Waves," *ACI Materials Journal*, V. 92, No. 5, Sept.-Oct. 1993, pp. 511-523.

8. Halabe, U. B.; Chenn, H.; Bhandarkar, V.; and Sami, Z., "Detection of Sub-Surface Anomalies in Concrete Bridge Decks Using Ground Penetrating Radar," *ACI Materials Journal*, V. 94, No. 5, Sept.-Oct. 1997, pp. 396-408.

9. Holt, F. B., and Eales, J. W., "Nondestructive Evaluation of Pavements," *Concrete International*, V. 9, No. 6, June 1997, pp. 41-45.

10. Chung, T.; Carter, C. R.; Masliwec, T.; and Manning, D. G., "Impulse Radar Evaluation of Asphalt-Covered Bridge Decks," *IEEE Transactions on Aerospace and Electronic Systems*, V. 28, No. 1, 1992, pp.125-136.

11. Chen, H. L. R.; Halabe, U. B.; Sami, Z.; and Bhandarkar, V., "Impulse Radar Reflection Waveforms of Simulated Reinforced Concrete Bridge Decks," *Materials Evaluation*, 1994, pp. 1388-1392.

12. Narayanan, R. M.; Hudson, S. G.; and Kumke, C. J., "Detection of Rebar Corrosion in Bridge Decks Using Statistical Variance of Radar Reflected Pulses," GPR 98, *Proceedings*, Seventh International Conference on Ground-Penetrating Radar, Lawrence, Kans., May 27-30, 1998, pp. 601-605.

13. Goodier, A.; Matthews, S. L.; and Massey, S., "Evaluating Structural Concrete Using Subsurface Radar, Concrete Durability and Repair Technology," *Proceedings of Creating with Concrete*, Dundee, Scotland, Sept. 1999, pp. 2-10.

14. Morey, R. M., "Ground Penetrating Radar for Evaluating Subsurface Conditions for Transportation Facilities," *Synthesis of Highway Practice 255*, National Cooperative/Highway Research Program, National Academy Press, Washington, D.C., 1998, 37 pp.

15. Scullion, T.; Lau, C.; and Chen, Y., "Implementation of the Texas Ground Penetrating Radar System," *Research Report* 1233-1, Texas Transportation Institute, 1994, 102 pp.

16. Maser, K. R., and Scullion, T., "Influence of Asphalt Layering and Surfacing Treatments on Asphalt and Base Layer Thickness Computations Using Radar," *Report* 1923-1, Texas Transportation Institute, 1992, 90 pp.

17. Annan, A. P., and Davis, J. L., "Radar Range Analysis for Geologic Materials," Report of Activities, *Geological Survey of Canada Paper* 77-713, 1997, pp. 117-124.

18. Zhang, J.; Monteiro, P. J. M.; and Morrison, F. H., "Non-Invasive Surface Measurement of Corrosion Impedance of Reinforcing Bar in Concrete—Part II: Forward Modeling," *ACI Materials Journal*, V. 99, No. 3, May-June 2002, pp. 242-249.

19. Annan, A. P., and Davis, J. L., "Impulse Radar Sounding in Permafrost," *Radio Science*, V. 11, No. 4, 1976, pp. 383-384.

20. Ulriksen, C. P. F., "Application of Impulse Radar to Civil Engineering," PhD thesis, Dept. of Engineering Geology, Lund University of Technology, Sweden, 1992.

21. Bracewell, R., *The Fourier Transform and Its Applications*, McGraw-Hill, New York, 1965, 381 pp.

22. Dagan, G., *Flow and Transport in Porous Media*, Springer-Verlag, New York, 1989, 461 pp.

23. Jones D. A., *Principles and Prevention of Corrosion*, 2nd Edition, Prentice Hall, 1992, 352 pp.

24. Gu, P.; Elliott, S.; Hristova R.; Beaudoin, J. J.; Brousseau, R.; and Baldock, B., "A Study of Corrosion Inhibitor Performance in Chloride Contaminated Concrete by Electrochemical Impedance Spectroscopy," *ACI Materials Journal*, V. 94, No. 5, Sept.-Oct. 1997, pp. 385-394.